Matching ASCAT and QuikSCAT winds

Abderrahim Bentamy,[1] Semyon A. Grodsky,[2] James A. Carton,[2] Denis Croizé-Fillon,[1] and Bertrand Chapron[1]

[1]   Surface winds from two scatterometers, the Advanced scatterometer (ASCAT), available since 2007, and QuikSCAT, which was available through November 2009, show persistent differences during their period of overlap. This study examines a set of collocated observations during a 13-month period November 2008 through November 2009, to evaluate the causes of these differences. A difference in the operating frequency of the scatterometers leads to differences that this study argues depend on rain rate, wind velocity, and SST. The impact of rainfall on the higher frequency QuikSCAT introduces biases of up to 1 m s^{-1} in the tropical convergence zones and along the western boundary currents even after rain flagging is applied. This difference from ASCAT is reduced by some 30% to 40% when data for which the multidimensional rain probabilities > 0.05 is also removed. An additional component of the difference in wind speed seems to be the result of biases in the geophysical transfer functions used in processing the two data sets and is parameterized here as a function of ASCAT wind speed and direction relative to the mid-beam azimuth. After applying the above two corrections, QuikSCAT wind speed remains systematically lower (by 0.5 m s^{-1}) than ASCAT over regions of cold SST < 5°C. This difference appears to be the result of temperature-dependence in the viscous damping of surface waves which has a greater impact on shorter waves and thus preferentially impacts QuikSCAT. The difference in wind retrievals also increases in the storm track corridors as well as in the coastal regions where the diurnal cycle of winds is aliased by the time lag between satellites.

Citation: Bentamy, A., S. A. Grodsky, J. A. Carton, D. Croizé-Fillon, and B. Chapron (2012), Matching ASCAT and QuikSCAT winds, *J. Geophys. Res.*, *117*, C02011, doi:10.1029/2011JC007479.

1.   Introduction

[2]   Many meteorological and oceanic applications require the high spatial and temporal resolution of satellite winds [e.g., *Grima et al.*, 1999; *Grodsky and Carton*, 2001; *Blanke et al.*, 2005; *Risien and Chelton*, 2008]. Many of these studies also require consistent time series spanning the lifetime of multiple satellite missions, of which there have been seven since the launch of the first European Remote Sensing satellite (ERS-1) in August 1991. Creating consistent time series requires accounting for changes in individual mission biases, most strikingly when successive scatterometers operate in different spectral bands [e.g., *Bentamy et al.*, 2002; *Ebuchi et al.*, 2002]. This paper presents a comparative study of winds derived from the matching of two such scatterometers: the C-band Advanced SCATterometer (ASCAT) on board Metop-A and the higher frequency Ku-band SeaWinds scatterometer onboard QuikSCAT.

[3] Scatterometers measure wind velocity indirectly through the impact of wind on the amplitude of capillary or near-capillary surface waves. This wavefield is monitored by measuring the strength of Bragg scattering of an incident microwave pulse. If a pulse of wave number k_R impinges on the surface at incidence angle θ relative to the surface the maximum backscatter will occur for surface waves of wave number $k_B = 2k_R \sin(\theta)$ whose amplitude, in turn, reflects local wind conditions [e.g., *Wright* and *Keller*, 1971]. The fraction σ^0 of transmitted power that returns back to the satellite is thus a function of local wind speed and direction (relative to the antenna azimuth), and θ.

[4] To date, the most successful conversions of scatterometer measurements into near-surface wind rely on empirically derived geophysical model functions (GMFs) augmented by procedures to resolve directional ambiguities resulting from uncertainties in the direction of wave propagation. Careful tuning of the GMFs is currently providing estimates of 10 m neutral wind velocity with errors estimated to be around $\pm$ 1 m s^{-1} and $\pm$ 20° [e.g., *Bentamy et al.*, 2002; *Ebuchi et al.*, 2002]. However, systematic errors are also present. For example, *Bentamy et al.* [2008] have shown that ASCAT has a systematic underestimation of wind speed that increases with wind speed, reaching 1 m s^{-1} for winds of 20 m s^{-1}.

[1]Institut Francais pour la Recherche et l'Exploitation de la Mer, Plouzane, France.
[2]Department of Atmospheric and Oceanic Science, University of Maryland, College Park, Maryland, USA.

Table 1. Orbital Parameters

Satellite	QuikSCAT	METOP-A
Recurrent period	4 days	29 days
Orbital period	101 min	101 min
Equator crossing local Sun time at ascending node	6:30 A.M.	9:30 A.M.
Altitude above equator	803 km	837 km
Inclination	98.62°	98.59°

[5] The GMFs and other parameters must change if the frequency band used by the scatterometer changes. Historically scatterometers have used two different frequency bands. U.S. scatterometers as well as the Indian OCEANSAT2 use frequencies in the 10.95–14.5 GHz Ku-band. In contrast the European Remote Sensing satellite scatterometers have all adopted the 4–8 GHz C-band to allow for reduced sensitivity to rain interference [*Sobieski et al.*, 1999; *Weissman et al.*, 2002]. To avoid spurious trends and variability in a combined multiscatterometer data set, the bias in wind and its variability between different scatterometers needs to be removed. This paper doesn't consider adjustment of wind variability.

[6] There have been numerous efforts to construct a combined multisatellite data set of winds [*Milliff et al.*, 1999; *Zhang et al.*, 2006; *Bentamy et al.*, 2007, *Atlas et al.*, 2011]. These efforts generally rely on utilizing a third reference product such as passive microwave winds or reanalysis winds to which the individual scatterometer data sets can be calibrated. In contrast to such previous efforts, this current study focuses on directly matching scatterometer data. We illustrate the processes by matching the current ASCAT and the recent QuikSCAT winds (following *Bentamy et al.* [2008]). This matching exploits the existence of a 13 month period November 2008 to November 2009 when both missions were collecting data and when ASCAT processing used the current CMOD5N GMF [*Verspeek et al.*, 2010] to derive 10 m neutral wind.

2. Data

[7] This study relies on data from two scatterometers, the SeaWinds Ku-band (13.4 GHz, 2.2 cm) scatterometer onboard QuikSCAT (referred to as QuikSCAT or QS, Table 1) which was operational June, 1999 to November, 2009 and the C-band ASCAT onboard the European Meteorological Satellite Organization (EUMESAT) MetOp-A (http://www.eumetsat.int/Home/Main/DataProducts/Atmosphere/index.htm) (5.225 GHz, 5.7 cm) launched October, 2006 (referred to as ASCAT or AS).

[8] QuikSCAT uses a rotating antenna with two emitters: the H-pol inner beam with an incidence angle $\theta = 46.25°$ and the V-pol outer beam with an incidence angle of $\theta = 54°$. Observations from these two emitters have swaths of 1400 km and 1800 km, respectively which cover around 90% of the global ocean daily. These observations are then binned into Wind Vector Cells (WVC). QuikSCAT winds used in this study are the 25-km Level 2b data produced and distributed by NASA/Jet Propulsion Laboratory, product ID is PODAAC-QSX25-L2B0 (http://podaac.jpl.nasa.gov/dataset/QSCAT_LEVEL_2B?ids=Measurement&values=Ocean%20Winds) [*Dunbar et al.*, 2006]. These data are estimated

with the empirical QSCAT-1 GMF and the Maximum Likelihood Estimator which selects the most probable wind direction. To improve wind direction estimates in the middle of the swath an additional Direction Interval Retrieval with Threshold Nudging algorithm is applied. The winds produced by this technique show RMS speed and direction differences from concurrent in situ buoy and ship data of approximately 1 m s^{-1} and 23°, and temporal correlations in excess of 0.92 [e.g., *Bentamy et al.*, 2002; *Ebuchi et al.*, 2002; *Bourassa et al.*, 2003].

[9] The QuikSCAT wind product includes several rain flags determined directly from scatterometer observations and from collocated radiometer rain rate measurements from other satellites. The impact of rain on QuikSCAT data is indicated by two rain indices: a rain flag and a multidimensional rain probability (MRP). All QuikSCAT retrievals identified as contaminated by rain are removed using the rain flag associated with each WVC. Additional rain selection is based on MRP index provided by the Impact-based Multidimensional Histogram technique. Employing MRP enhances rain selection since 'rain free' pixels identified with the rain flag index not always have MRP = 0. Recently the JPL/PODAAC has reprocessed QuikSCAT data using the new Ku-2011 GMF [*Ricciardulli and Wentz*, 2011] (see also www.ssmi.com/qscat/qscat_Ku2011_tech_report.pdf). Preliminary analysis of this product indicates improvements in the tropical rainfall detection, but major differences between QuikSCAT and ASCAT winds reported below do not change much.

[10] ASCAT has an engineering design that is quite different from QuikSCAT. Rather than a rotating antenna it has a fixed three beam antenna looking 45° (fore-beam), 90° (mid-beam), 135° (aft-beam) of the satellite track, which together sweep out two 550 km swaths on both sides of the ground track. The incidence angle varies in the range 34°–64° for the outermost beams and 25°–53° for the mid-beam, giving Bragg wavelengths of 3.2–5.1 cm and 3.6–6.8 cm, respectively. Here we use Level 2b ASCAT near real-time data (version 1.10) distributed by EUMETSAT and by KNMI at 25×25 km^2 resolution. Comparisons to independent mooring and shipboard observations by *Bentamy et al.* [2008] and *Verspeek et al.* [2010] show that ASCAT wind speed and direction has accuracies similar to QuikSCAT.

[11] Rain contamination in the C–band, used by ASCAT, is weaker than in the Ku-band [e.g. *Tournadre and Quilfen*, 2003]. The selection of ASCAT retrievals is based on the quality control flag associated with each WVC. All quality flag bits, including rain flag but excluding strong wind (>30 m s^{-1}) and weak wind (<3 m s^{-1}) flags, are checked to be 0.

[12] To reevaluate wind accuracy we use a variety of moored buoy measurements including wind velocity, SST, air temperature, and significant wave height. These are obtained from Météo-France and U.K. MetOffice (European seas) [*Rolland and Blouch*, 2002], the NOAA National Data Buoy Center (NDBC, U.S. coastal zone) [*Meindl and Hamilton*, 1992], and the tropical moorings of the Tropical Atmosphere Ocean Project (Pacific), the Pilot Research Moored Array (Atlantic), and Research Moored Array for African-Asian-Australian Monsoon Analysis and Prediction project (Indian Ocean) [*McPhaden et al.*, 1998; *Bourlès et al.*, 2008; *McPhaden et al.*, 2009]. Hourly averaged
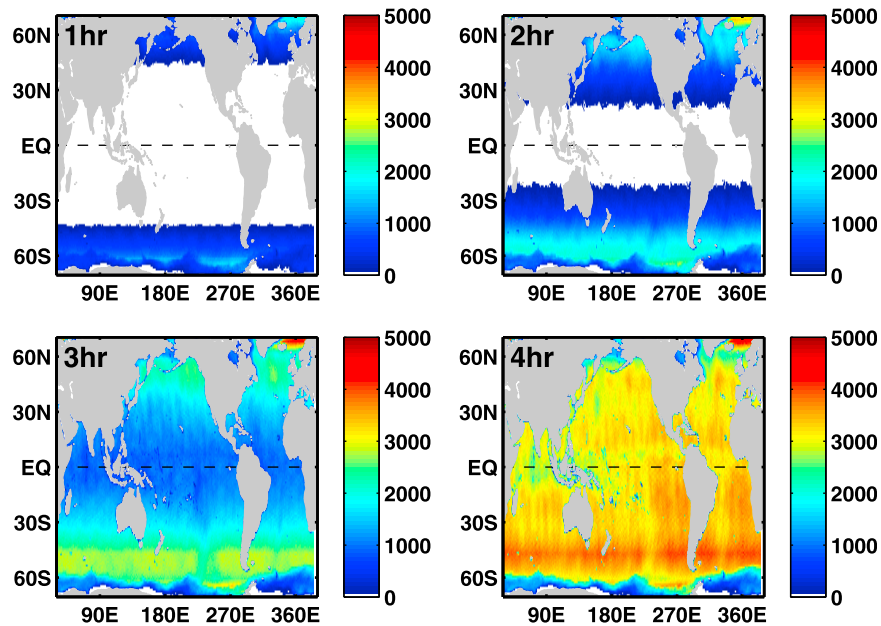
Figure 1. Number of collocated QuikSCAT and ASCAT data on a 1° × 1° grid during November 2008–2009 for time separations less than that shown in the top left corner.

post-processed (off-line) buoy measurements of wind velocity, sea surface and air temperatures, and humidity are converted to neutral wind at 10 m height using the COARE3.0 algorithm of *Fairall et al.* [2003]. Although this algorithm allows for the use of surface wave and currents data, we do not include the corrections since these data are not available for most buoys.

[13] Quarter-daily 10 m winds, as well as SST and air temperatures, are also obtained from the European Centre for Medium Weather Forecasts (ECMWF) operational analysis. These are routinely provided by the Grid for Ocean Diagnostics, Interactive Visualization and Analysis (GODIVA) project (http:// behemoth.nerc-essc.ac.uk/ncWMS/godiva2. html) on a regular grid of 0.5° in longitude and latitude.

3. Collocated Observations

[14] Both satellites are in quasi sun-synchronous orbits, with the QuikSCAT local equator crossing time at the ascending node (6:30 A.M.) leading the ASCAT local equator crossing time (9:30 A.M.) by 3 h. This difference implies that data precisely collocated spatially are available only with a few hours time difference at low latitudes (Figure. 1) [*Bentamy et al.*, 2008]. Here we accept for examination data pairs collocated in space and time where QuikSCAT WVC is collected within $0 < \tau < 4$ h and 50 km of each valid ASCAT WVC. For the thirteen month period November 2008 through November 2009 this collocation selection procedure produces an average 2800 collocated pairs of data in each 1° × 1° geographical bin. The data count is somewhat less in the regions of the tropical convergence zones due to the need to remove QuikSCAT rain flagged data. The data count increases with increasing latitude as a result of the near-polar orbits, but decreases again at very high latitudes due to the presence of ice. At shorter lags of $\tau <$ 3 h collocated data coverage is still global, but the number

of match-ups is reduced by a factor of two. At lags of $\tau <$ 1 h collocated data is only available in the extra tropics (Figure 1).

[15] Systematic difference in times of QuikSCAT and ASCAT overpasses may project on the diurnal variations of winds, and thus may result in nonzero time mean wind difference between the two satellites. This possible difference is addressed by examining sub-sampled buoy and ECMWF analysis data. Results of this examination are explained, but not shown, below. In midlatitudes, where the characteristic time separation between collocated ASCAT and QuikSCAT data is less than 2 h, we examine wind measurements from NDBC buoys. We subsample the original buoy data based on the timing of the nearest ASCAT (subsample 1, 'ASCAT') and QuikSCAT (subsample 2, 'QuikSCAT') overpasses. The time mean bias between wind speed subsamples at these extra-tropical NDBC mooring locations is close to zero with an RMS difference of less than 1 m s^{-1}, and a temporal correlation > 0.95. Time mean difference (bias) in wind speed between these 'QuikSCAT' and 'ASCAT' subsamples does not depend on wind strength and/or buoy location, and varies between ±0.1 m s^{-1} in 92% of cases. This negligible time mean bias suggests that time mean differences between collocated satellite wind fields (if any) are the result of differences in the satellite wind estimates rather than the time lag between samples. Similar results are found in a comparison of 'QuikSCAT' and 'ASCAT' subsamples of the tropical moorings (assuming $\tau < 4$ h). Again we find no mean bias, RMS differences of 1.2 m s^{-1}, and temporal correlations > 0.92. Finally we examine the impact of our choice of collocation ranges by simulating the space and time sampling of ASCAT and QuikSCAT with ECMWF analysis surface winds during the period November 20, 2008 through November 19, 2009. This sampling study confirms that the time lag between the two satellites doesn't produce any significant geographical patterns of wind speed bias. (A report is
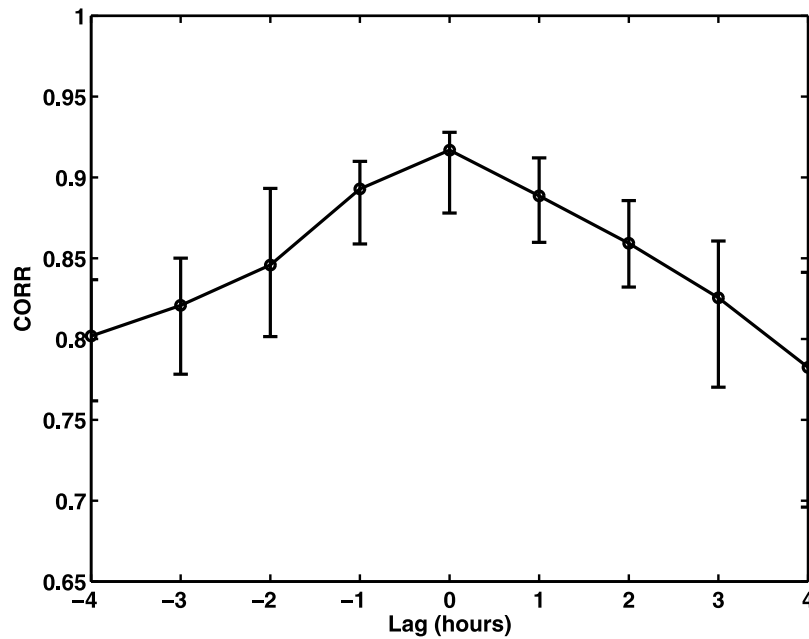
Figure 2. Lagged correlation of collocated satellite and buoy winds as a function of time separation between satellite and buoy data. Solid line shows the median value and vertical bars are bounded by 25th and 75th percentiles of correlation for different buoys.

available at http://coaps.fsu.edu/scatterometry/meeting/docs/2011/cal_val/Bentamy_Grodsky_IOVWST_2011.pdf.)

[16] Temporal correlation of satellite and the tropical buoy winds is high for all of our accepted time lags (Figure 2). It is close to 0.8 at $\tau = 4$ h (3–4 h is the most frequent time lag for ASCAT-QuikSCAT collocations in the tropics), but exceeds 0.9 at zero lag. At higher latitudes, where the winds have longer synoptic timescales, the collocated satellite-buoy time series have even higher correlations (0.89 at $\tau = 4$ h, and 0.96 at $\tau < 0.5$ h, not shown).

4. Results

4.1. Global Comparisons

[17] Time mean difference between collocated QuikSCAT and ASCAT wind speed ($\Delta W = W_{QS} - W_{AS}$, Figure 3) is generally less than 1 m s^{-1}, but contains some planetary-scale patterns. In general, $\Delta W > 0$ at tropical to midlatitudes where it exhibits a pattern of values in the range of 0.40–0.80 m s^{-1}, exceeding the bias found by *Bentamy et al.* [2008] between ASCAT and buoy winds, and resembling the spatial pattern of tropical and midlatitude storm track precipitation. This spatial pattern suggests that even after applying the rain flag to exclude rain-contaminated observations there is a residual impact of rainfall on QuikSCAT wind retrievals, as previously noted by, e.g., *Weissman et al.* [2002]. Enhancing rain flagging by removing cases with MRP > 0.05 (5% of QuikSCAT data) decreases the frequency of positive differences in the tropical precipitation zones by some 30% to 40% and reduces the number of large differences |ΔW| > 1 m s^{-1} by 38% (Figures 3a and 3b). However, the RMS variability of ΔW doesn't change with the enhanced rain flagging. Both with and without additional rain flagging RMS(ΔW) has a maximum of up to 3 m s^{-1} in the zones of the midlatitude storm tracks of both hemispheres

and approaches 1.8 m s^{-1} in the tropical convergence zones (Figures 3c and 3d). These maxima in inter-instrument variability reflect a combination of still unaccounted impacts of rain events, and impacts of strong transient winds in the midlatitude storm tracks, as well as deep convection events in the tropics. Still, because it removes extreme differences, this enhanced rain flagging is applied to all QuikSCAT data shown below.

[18] In contrast to the tropics or midlatitudes, time mean ΔW is negative at subpolar and polar latitudes. This is particularly noticeable at southern latitudes where the difference may exceed -0.5 m s^{-1}. This striking high latitude inter-scatterometer difference remains even after applying the enhanced rain flagging mentioned above (Figures 3a and 3b).

[19] Despite these time-mean differences the temporal correlation of QuikSCAT and ASCAT winds is high (>0.9) over much of the global ocean (Figures 3e and 3f). It decreases to 0.7 (0.5 at some locations) in the tropical convergence zones at least in part because of the relatively large noise compared to the wind signal (sampling errors due to unresolved tropical convection, weak winds variability) results in reduced correlation [*Bentamy et al.*, 2008]. An additional factor is the presence of mesoscale wind disturbances due to transient deep convective systems. The limited spatial scales of transient winds associated with the tropical convection approach the scale of a single radar footprint while their temporal scales approach the time lag between the two satellites [*Houze and Cheng*, 1977]. In contrast, the correlation at mid and high latitudes is high because winds there have long multiday synoptic timescales and large spatial scales.

4.2. Effect of Geophysical Model Function

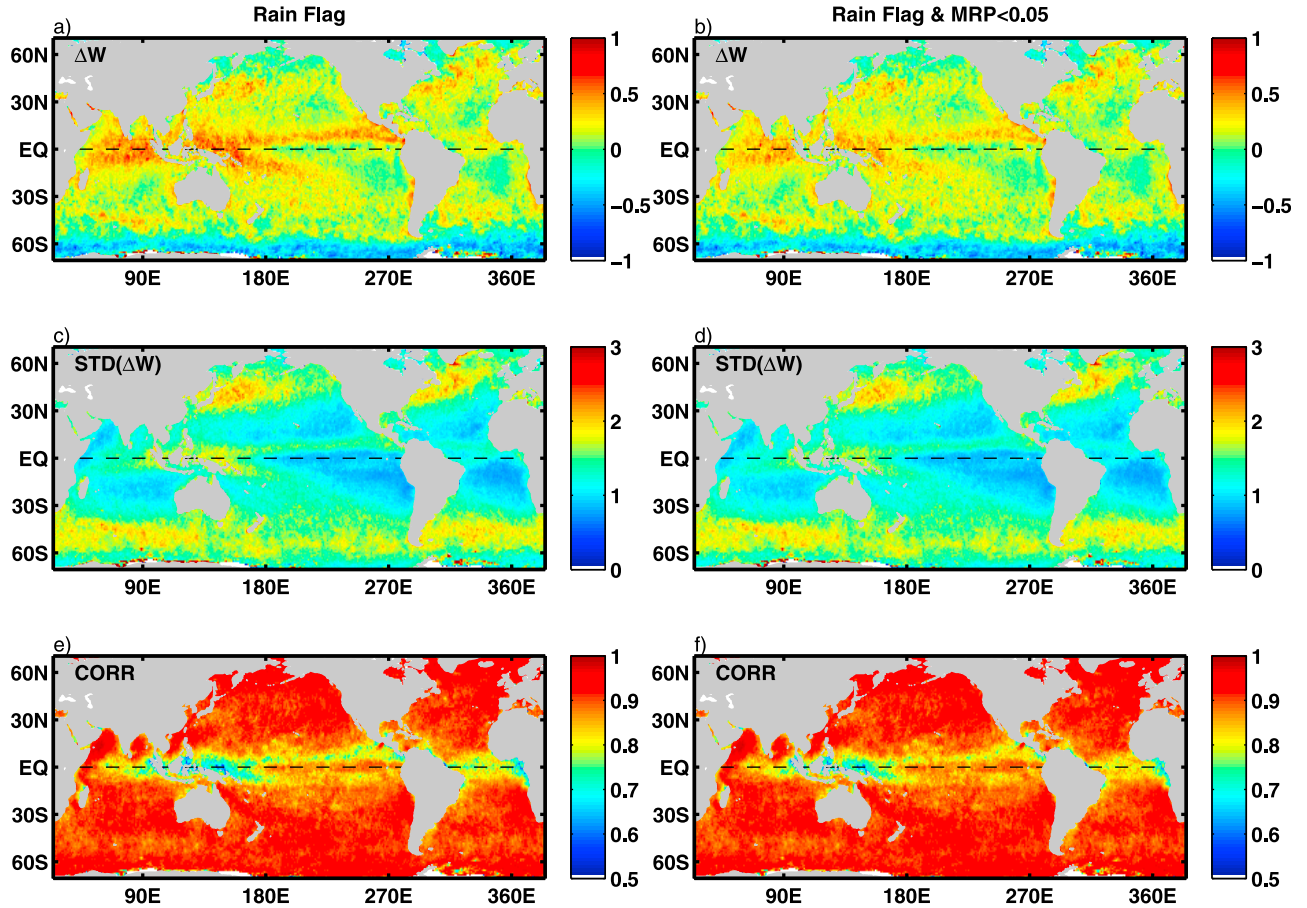[20] In this section we attempt to parameterize observed ΔW (after applying enhanced rain flagging to the QuikSCAT

Figure 3. Time mean (November 2008 to November 2009) difference between collocated QuikSCAT and ASCAT wind speed (ΔW), their standard deviation (STD), and temporal correlation (CORR). (left) Only rain flag is applied to QuikSCAT, and (right) rain flag and multidimensional rain probability (MPR < 0.05) are both applied.

data) as a function of geophysical and satellite-earth geo-metrical factors. The ASCAT GMF is parameterized by a truncated Fourier series of wind direction (DIR) relative to antenna azimuth (AZIM) for each of the antenna beams $\chi =$ DIR-AZIM as

$$\sigma^0 = B_0 + B_1 \cos\chi + B_2 \cos2\chi, \qquad (1)$$

where the coefficients B depend on wind speed and incident angle, θ. This suggests that a correction function dW (to be added to ASCAT winds in order to adjust them to QuikSCAT winds) should depend on similar parameters, $dW(W_{AS}, \chi, \theta)$. Due to the fixed, three beam observation geometry of ASCAT, the azimuthal dependence of dW is reduced to dependence on ASCAT wind direction relative to the ASCAT mid-beam azimuth, $\varphi = DIR_{AS} - AZIM_1$.

[21] Empirical estimates of this correction function dW are constructed by binning observed ΔW and wind direction difference as a function of wind speed, φ, and θ. Here we begin by considering estimates based on data from latitudes equatorward of 55° where the time mean ΔW values are mostly positive. Figure 4a reveals a clear dependence of ΔW on ASCAT wind speed. In agreement with the previous assessment of *Bentamy et al.* [2008] ASCAT wind speed is

consistently lower than QuikSCAT wind speed for $W_{AS} >$ 15 m s^{-1} (Figure 4a). The difference also apparent for $W_{AS} <$ 3 m s^{-1} is artificial and results from asymmetrical distribution of wind speed sampling for winds approaching the low wind speed cutoff [*Freilich*, 1997]. Binning ΔW versus ASCAT mid-beam incident angle (Figure 4b) shows only a weak dependence on θ. This implies that ΔW averaged over the whole range of azimuth and wind speed does not depend on the ASCAT incidence angle. Indeed, previous studies [e.g., *Bentamy et al.*, 2008; *Verspeek et al.*, 2010] have indicated that ASCAT wind speed distributions are not incidence angle dependent. Although it does not verify that the dependence of ΔW on θ can be ignored at any specific W_{AS} and φ, we assume that incidence angle may be eliminated from fitting parameters of the correction function dW.

[22] Wind direction retrievals from QuikSCAT and ASCAT, in contrast, do not show any dependence on ASCAT wind speed, θ, and relative wind direction φ (Figure 5). Interesting, although the mean wind directions agree well, their standard deviation does increase at low winds (Figure 5a). There are a number of possible reasons for this including the presence of variability at low wind speeds that is not resolved by the collocation criteria in space and/or time as well as wind retrieval issues. One of wind retrieval
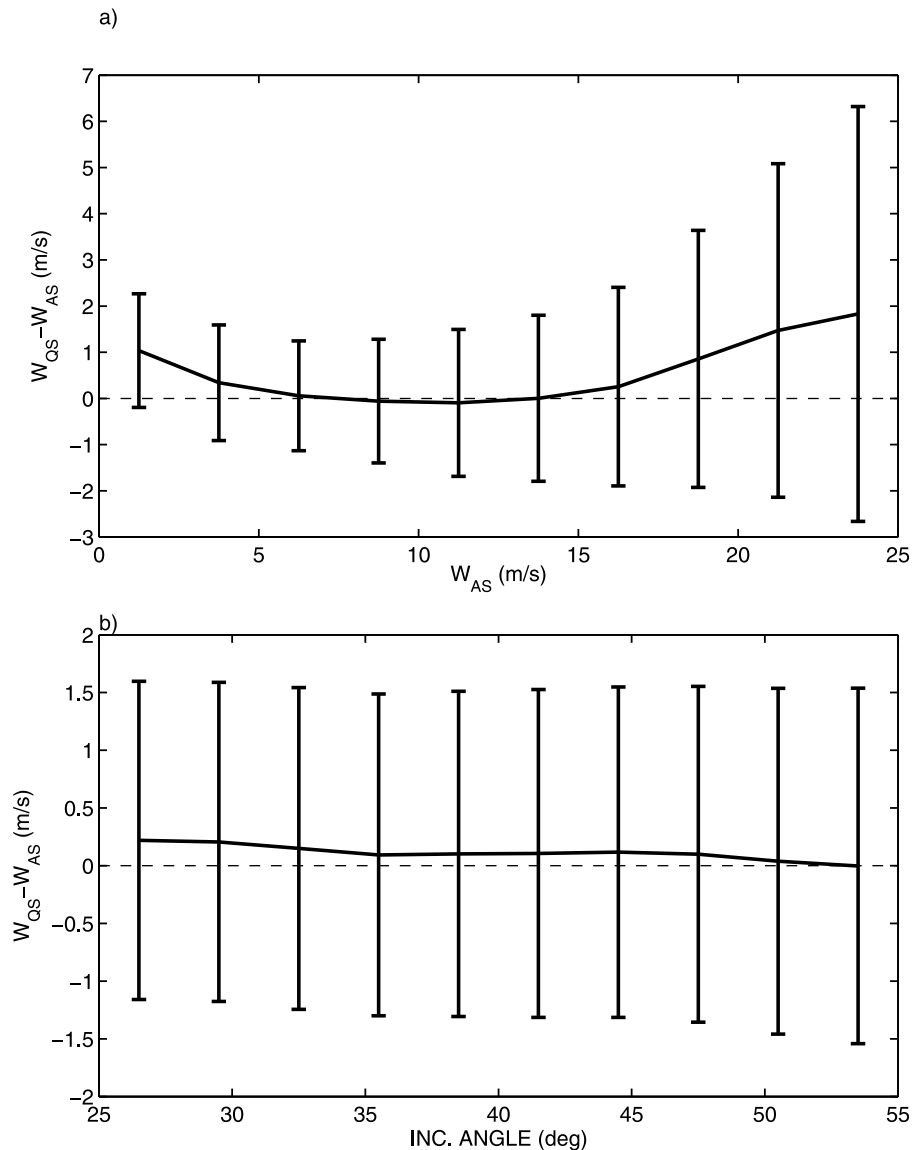
a)

b)

Figure 4. Difference between collocated wind speed from QuikSCAT (QS) and ASCAT (AS) binned versus (a) ASCAT wind speed and (b) ASCAT mid-beam incident angle. The error bars are the standard deviation of data in 2 m s^{-1} and 2° bins for Figure 4a and Figure 4b, respectively.

issues that lead to spurious wind direction preferences with respect to the ASCAT antenna azimuth has been recently described by *Ebuchi* [2011].

[23] There is also a clear dependence of QuikSCAT-minus-ASCAT wind speed difference on φ, again suggesting errors in ASCAT GMF (the QuikSCAT error must not be associated with ASCAT since the QuikSCAT data is independent of the azimuthal orientation of the ASCAT beams). For the ASCAT mid-beam looking in the wind vector direction ($\varphi = 0°$) ΔW is small. Looking in the upwind direction ($\varphi = \pm180°$) QuikSCAT wind speed is stronger than ASCAT by 0.5 m s^{-1}. Looking in the cross-wind direction ($\varphi = \pm90°$) ASCAT wind speed is stronger than QuikSCAT wind speed by approximately 0.2 m s^{-1}. Similar azimuthal dependencies show up in the difference between

buoy wind speed and ASCAT wind speed (Figure 7) although the data scatter is larger due to the smaller number of satellite-buoy collocations (compare right hand axes in Figures 6 and 7).

[24] We next examine the dependence of ΔW on both wind speed and azimuth (Figure 8). For all wind directions, QuikSCAT exceeds ASCAT wind speed at both low ($W_{AS} < 3$ m s^{-1}) and high ($W_{AS} > 15$ m s^{-1}) winds, with a larger difference at high winds [see also *Bentamy et al.*, 2008]. For all wind speeds, QuikSCAT wind is stronger than ASCAT if the ASCAT mid-beam is oriented in the upwind direction ($\varphi = \pm180°$, compare with Figure 6). Binned data in Figure 8a are shown for the latitude band 55°S −55°N, thus excluding high latitude areas of negative ΔW (see Figure 5). Similar assessment of ΔW based on data from high southern
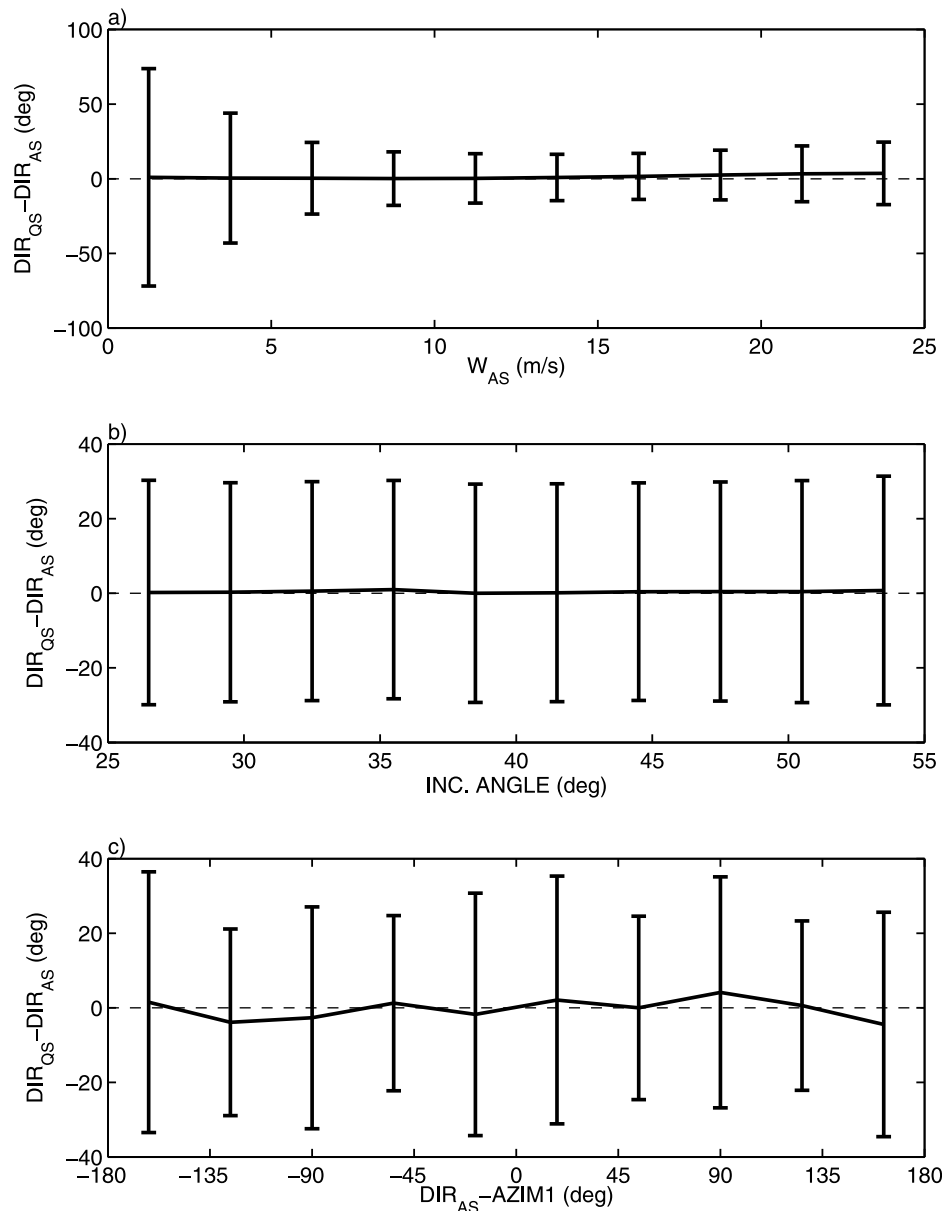
Figure 5. Difference between collocated wind direction from QuikSCAT (QS) and ASCAT (AS) binned versus (a) ASCAT wind speed, (b) ASCAT mid-beam incident angle, and (c) ASCAT wind direction relative to the mid-beam azimuth (zero corresponds to wind direction coinciding with the mid-beam azimuth). The error bars are the standard deviation of binned data.

latitudes only (south of 55°S) has similar dependence on wind speed and azimuth but stronger negative ΔW at winds below 15 m s^{-1} (Figure S1 in the auxiliary material).[1]

[25] Most of collocated data are collected at moderate winds between 5 m s^{-1} and 15 m s^{-1}, at which number of data in each bin exceeds $n = 10^5$/bin (Figure 8a). It decreases to $n = 10^4$/bin at $W_{AS} < 5$ m s^{-1} and drops below $n = 10^3$/bin at high winds $W_{AS} > 20$ m s^{-1}. Because of limited samples, binned ΔW are noisy at high winds and are not symmetrical in azimuth (Figure 8a). To mitigate the impact of sampling

errors we represent dW by its mean and first three symmetric harmonics

$$dW = \sum_{m=0}^{m=3} P_5^m(W_{AS})\cos(m\varphi), \qquad (2)$$

where the coefficients $P_5^m(W_{AS})$ are assumed to be fifth order polynomials of ASCAT wind speed. The polynomial coefficients in turn are estimated by least squares minimization (Table 2).

[26] To evaluate the usefulness of this approximation we compare its time mean structure to that of the time mean of
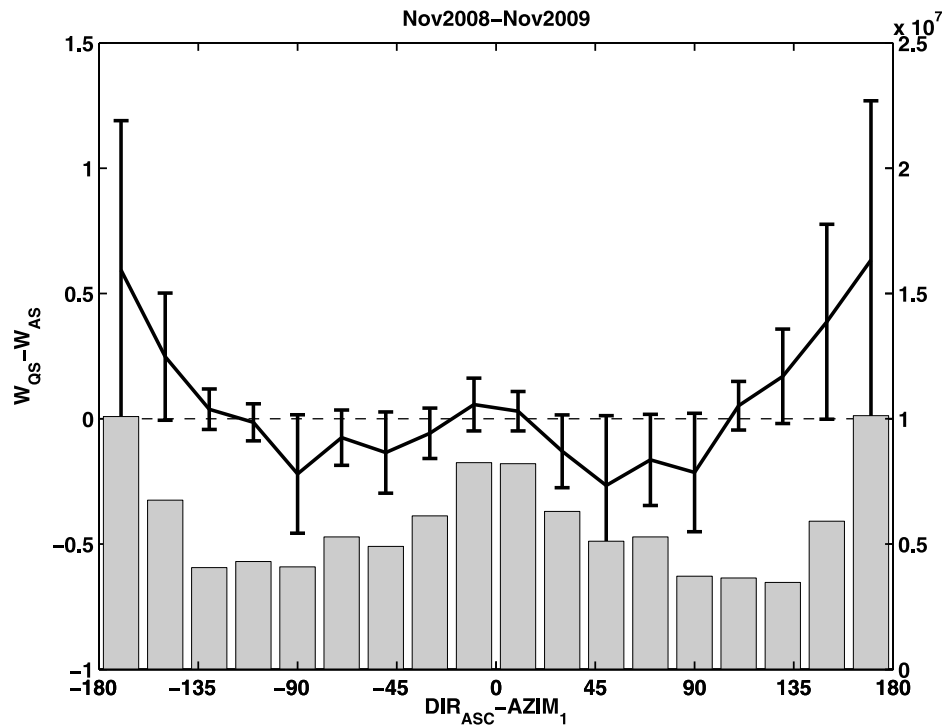
Figure 6. Difference between collocated QuikSCAT (QS) and ASCAT (AS) wind speed as a function of ASCAT wind direction relative to the mid-beam azimuth (DIR_{ASC}-$AZIM_1$). Data is averaged for all wind speeds and binned into 10° bins in the relative wind direction. The downwind direction corresponds to 0°. Wind direction histogram (gray, scale on right axis). The error bars are the standard deviation of binned data.
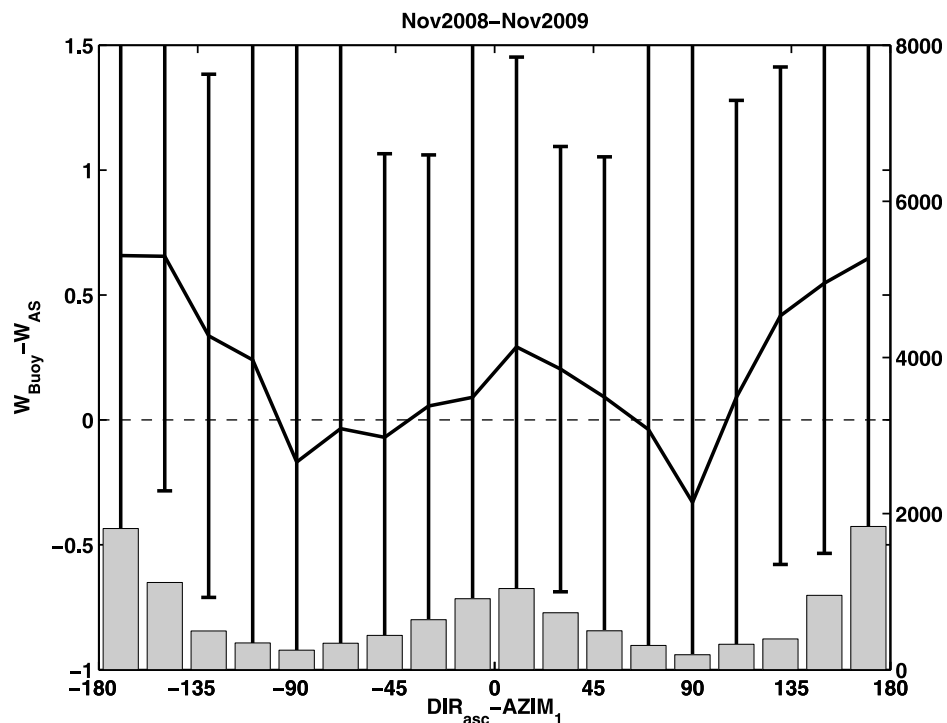

Figure 7. The same as in Figure 6, but for buoy minus ASCAT collocated wind speed differences.
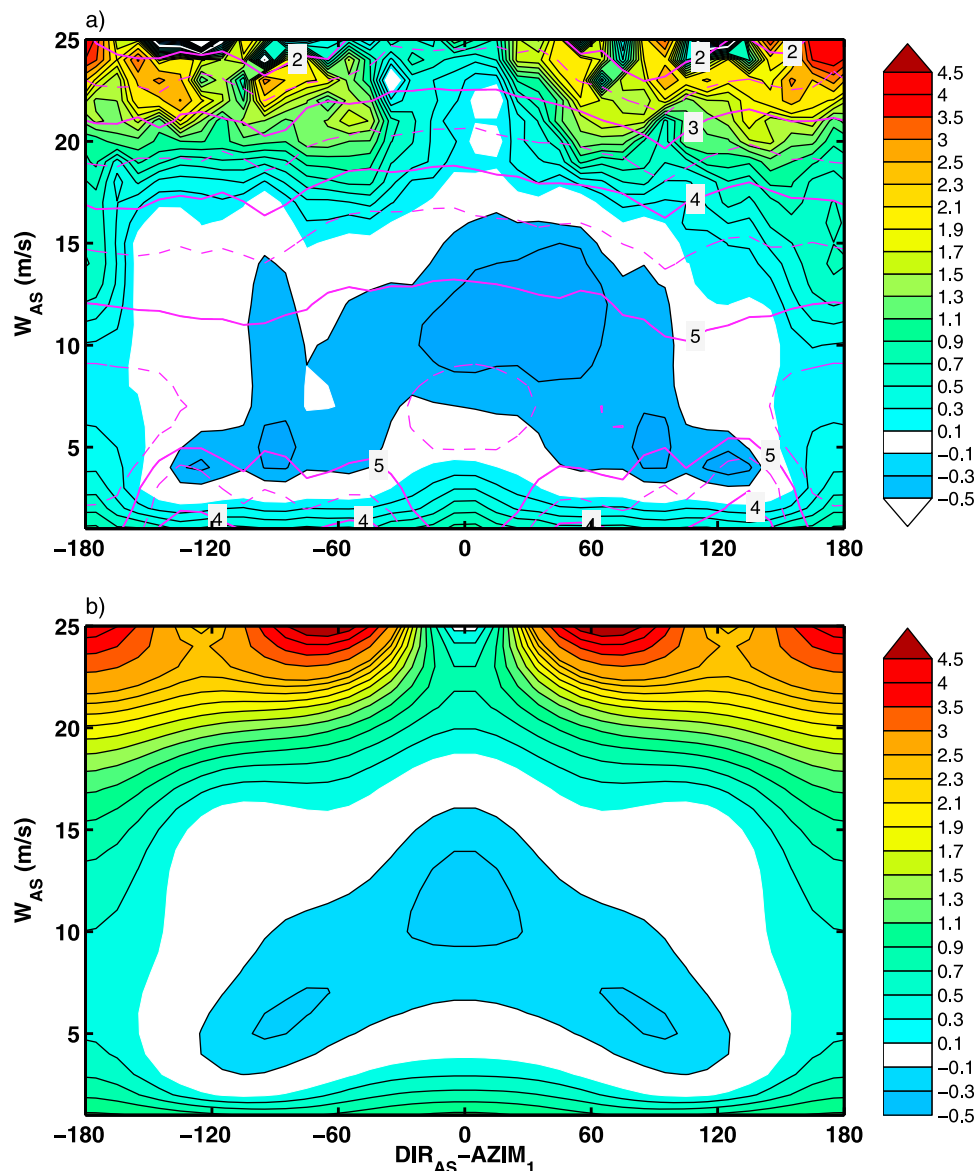
Figure 8. Collocated QuikSCAT-ASCAT neutral wind speed difference (m s^{-1}) binned into 1 m s^{-1} by 10° bins in ASCAT wind speed and wind direction relative to the ASCAT mid-beam azimuth $\varphi = DIR_{AS} - AZIM_1$. (a) Binned data, in the latitude band 55°S −55°N, thus excluding high latitude areas of negative ΔW (see Figure 5). (b) Data fit by equation (2). Number of data in each bin, $\log_{10}(n)$, is overlain by magenta contours in Figure 8a.

ΔW in Figure 9. This comparison shows that most of the spatial structure in the time mean of ΔW is retained in the time mean of dW. Applying the correction function (2) to instantaneous ASCAT winds leads to apparent decrease in the residual time mean wind speed difference (compare $W_{QS} - W_{AS}$ and $W_{QS} - W_{AS} - dW$ plots in Figure 9). The unmodeled time mean difference includes positive values in the regions of the midlatitude storm tracks, which is to be expected because ASCAT underestimates strong winds (>20 m s^{-1}). Strong wind events are relatively rare, and the correction function dW is uncertain at those conditions (Figure 8a). Some unmodeled time mean dW is also present in coastal areas such as off Peru and Namibia, where we suspect there are sampling problems resulting from under-resolving of the prominent diurnal land-sea breezes.

Table 2. Coefficients a_i^m of $P_5^m(W_{AS}) = \sum_{i=0}^{5} a_i^m (W_{AS})^i$ in (2) Which Parameterize the Difference Between QuikSCAT and ASCAT Wind Speeds in Terms of ASCAT Wind Speed W_{AS} and Wind Direction Relative to ASCAT Mid-beam Azimuth φ^a

	1	$\cos \varphi$	$\cos 2\varphi$	$\cos 3\varphi$	Factor
1	1.6774	0.1427	0.0894	0.2229	x 1
W_{AS}	−0.7974	0.2091	0.2806	−0.2903	x 1
W_{AS}^2	1.3854	−0.7235	−0.6268	0.8371	x 0.1
W_{AS}^3	−1.1416	0.7916	0.5320	−0.9592	x 0.01
W_{AS}^4	0.4476	−0.3579	−0.1906	0.4681	x 1e-3
W_{AS}^5	−0.6307	0.5709	0.2322	−0.8181	x 1e-5

[a]Columns represent coefficients a_i^m for angular harmonics $\cos(m\varphi)$ in (2), m = 0,1,2,3.
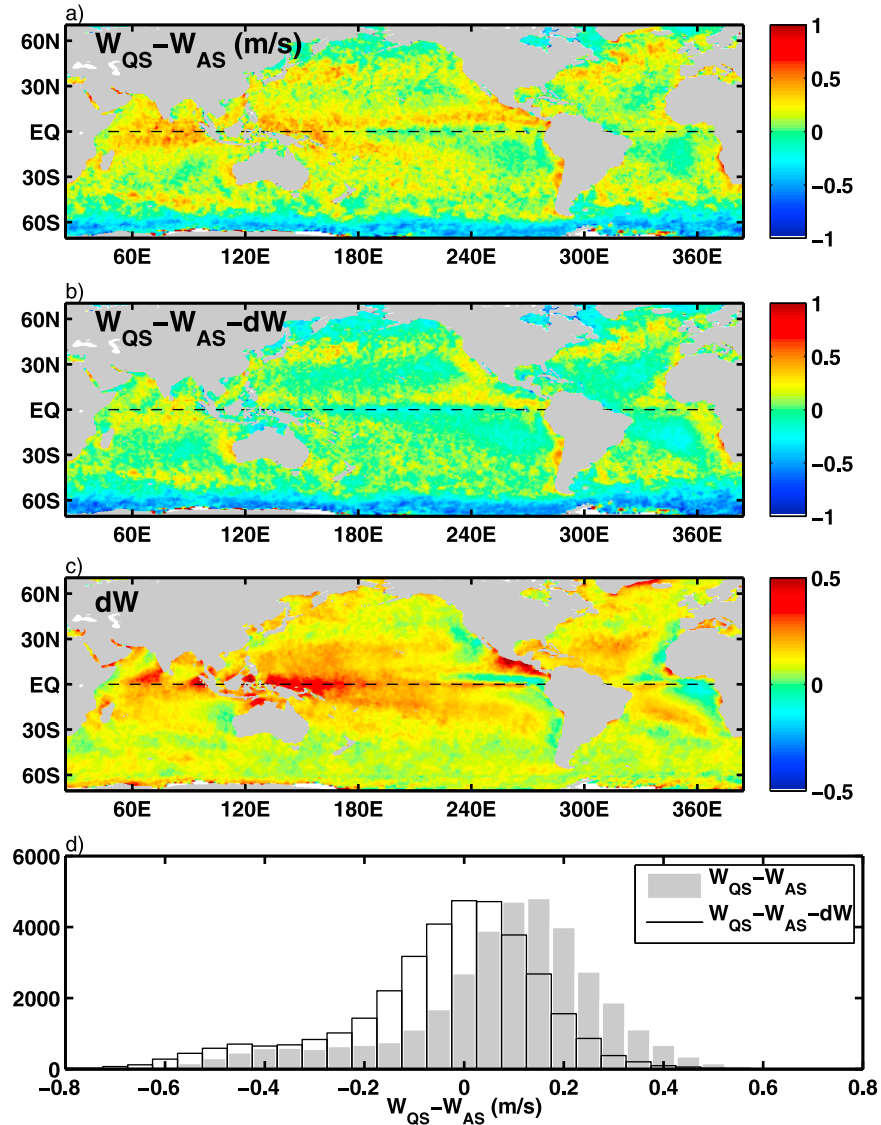
Figure 9. (a) Wind speed difference ($W_{QS} - W_{AS}$). (b) Wind speed difference after applying the correction function $dW(W_{AS}, \varphi)$. (c) Spatial distribution of time mean dW. (d) Histogram of wind speed difference before (gray) and after (outline) applying dW.

[27] After correction for our modeled dW the global histogram of $\Delta W = W_{QS} - W_{AS}$ eliminates the slight 0.18 m s^{-1} positive bias in ΔW (Figure 9). However, large negative tails of the distribution remain, reflecting the presence of large negative values of ΔW at high latitude mentioned previously. Here we explore a physically based hypothesis for this high latitude negative ΔW.

4.3. Impact of SST

[28] As described in Appendix A radar backscatter σ^0 depends on the spectrum of the resonant Bragg waves. These near-capillary waves have amplitudes that depend on a balance of wave growth and viscous dissipation, and the latter is a function of SST because of the impact of SST on viscosity. We present a linearized form of the dependence of ΔW on SST through a Taylor series expansion of the growth-dissipation equation around the space-time mean value of SST ($T_0 = 19°C$)

$$\delta W = -\frac{2[\nu(T) - \nu(T_0)](\omega_{QS} - \omega_{AS})}{(\rho_a/\rho_w)C_\beta C_D W(1 - \alpha_c)} \quad (3)$$

where the notation and variable definitions are given in Appendix A. δW is thus linearly dependent on the change in kinematic viscosity $\Delta \nu = \nu(T) - \nu(T_0)$ due its SST-dependence, inversely dependent on wind speed, and air density ρ_a. These dependencies are likely only important at high latitudes due to the temperature-dependent impact of kinematic viscosity (Figures 10b and 10d). According to (3), the magnitude of δW enhances south of 60°S (Figure 10d) due to the combination of cold SSTs (Figure 10b) and relatively weak winds (Figure 10a).
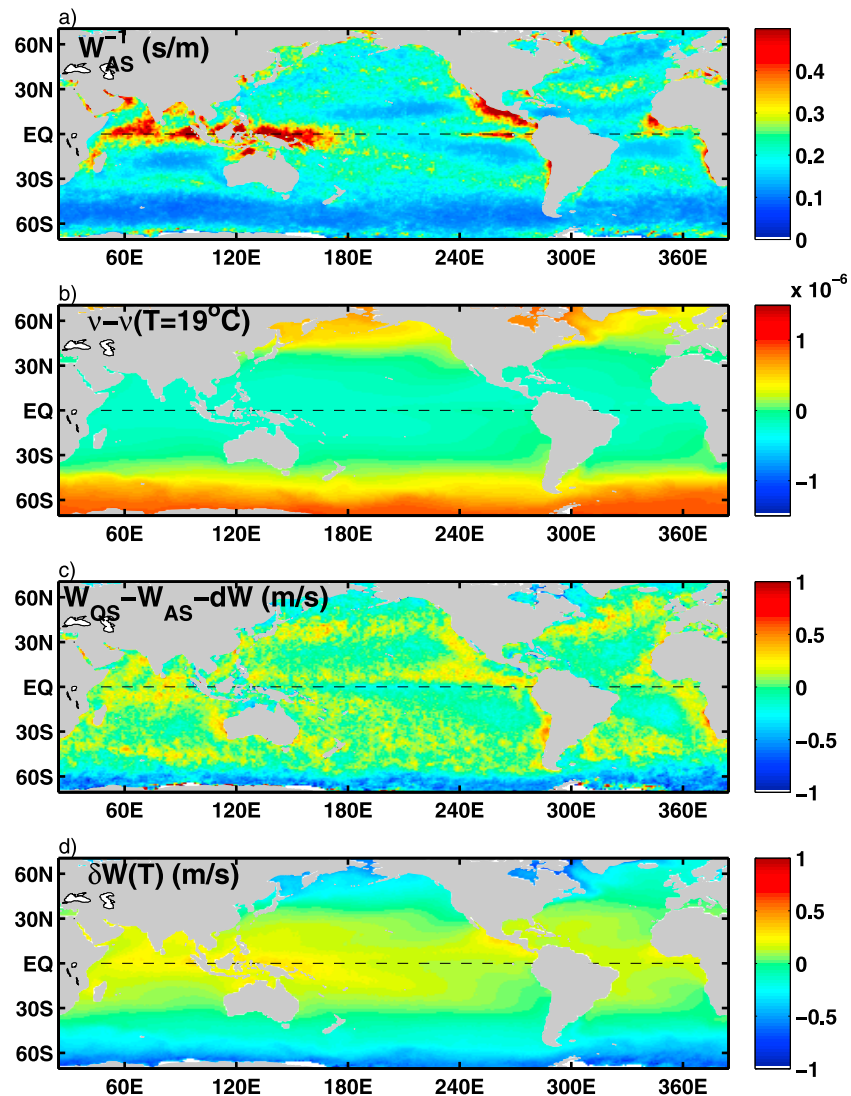
Figure 10. (a) Time mean inverse wind speed from ASCAT, W_{AS}^{-1}. (b) Difference in kinematic viscosity ($m^2\ s^{-1}$) of the seawater relative to the viscosity evaluated at global mean SST (19°C). (c) QuikSCAT-ASCAT wind speed difference after applying the correction function dW (the same as in Figure 9). (d) SST dependent difference between QuikSCAT and ASCAT wind speed $\delta W(T)$ based on (3) evaluated at $\theta = 45°$.

[29] SST-based interpretation of ΔW (Figure 10c) is in partial contradiction with the preferable occurrence of the negative wind speed difference at high south latitudes in comparison with the north. But cold SSTs < 5°C are present south of 60°S year around in distinction from the high northern latitudes where SSTs < 5°C are present only in boreal winter [see, e.g., *Locarnini et al.*, 2010] (see also http://www.nodc.noaa.gov/cgi-bin/OC5/WOA09F/woa09f.pl?parameter=t). But the seasonal presence of sea ice at high northern latitudes reduces the number of wind retrievals in boreal winter. This is one possible explanation of the south-north asymmetry in the time mean ΔW.

[30] An alternative explanation of the negative ΔW at high southern latitudes may involve impacts of anomalously strong waves. But closer examination of Figure 10c indicates that area of negative ΔW is displaced southward of the 'roaring forties' belt toward higher latitudes where SST is really cold (indirectly reflected in spatial variations of $\nu(T)$ in Figure 10b) but winds and waves are not that strong as to the north (Figure 10a).

[31] To summarize the impact of SST and winds on ΔW, on which (3) depends, we present the QuikSCAT minus ASCAT collocated differences binned as a function of wind speed and SST in Figure 11. Here 10-m wind speed and SST bins are determined from ECMWF analysis data collocated in space and time with satellite retrievals. Observed QuikSCAT wind speed is higher than ASCAT at low (<3 m s^{-1}) and high (>12 m s^{-1}) winds (Figure 11a). In contrast, ASCAT exceeds QuikSCAT wind speed by at least 0.25 m s^{-1} over cold SST < 7°C under moderate wind 5 m s^{-1} < W < 12 m s^{-1}. The most notorious positive ΔW is observed at high winds where W_{QS} exceeds W_{AS} by up to 2 m s^{-1}. These positives values we previously attributed to the difference in GMFs (see discussions surrounding
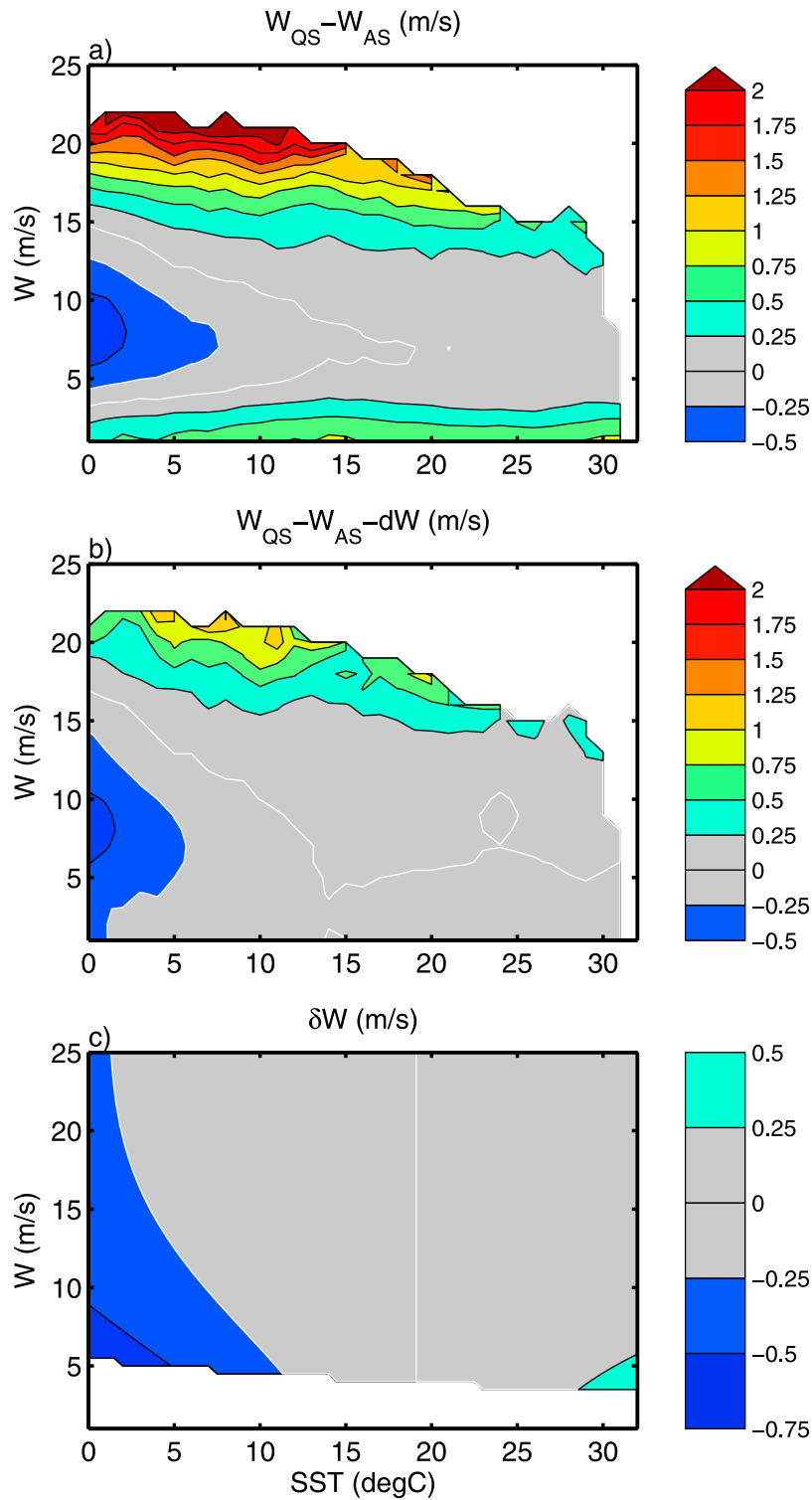
Figure 11. Collocated QuikSCAT-ASCAT neutral wind speed difference ($W_{QS} - W_{AS}$) binned 1° in SST and 1 m s^{-1} in wind speed from the ECMWF analysis collocated data: (a) observed data with MRP < 0.05 and (b) data after applying (2). Each bin contains an average 128,000 collocations. Bins with less than 2,000 collocations are blanked. (c) SST dependent QuikSCAT-ASCAT wind speed difference δW evaluated from (3) at $\theta = 45°$. Winds below the threshold wind (at which energy gain from wind is equal to viscous dissipation, $\beta_w - \beta_\nu = 0$) are blanked in Figure 11c.

Figure 8) are not explained by (3). Correction of ASCAT wind speed by (2) reduces ΔW at high winds but doesn't eliminate the deviation completely (compare Figures 11a and 11b). The strongest negative wind speed difference between the scatterometers is found at cold SST < 5°C. In contrast to the simple model in (3) comparison of Figures 11b and 11c shows that the negative difference between QuikSCAT and ASCAT wind speeds rises in magnitude for moderate winds while (3) implies that the strongest negative values should occur for weak winds. Examination of this discrepancy likely requires an improved parameterization of the wind-wave growth parameter and a more detailed radar imaging model. In particular we note that weak winds may act to dissipate rather than strengthen the centimeter-scale waves (see *Kudryavtsev et al.* [2005] for further details).

5. Summary

[32] The end of the QuikSCAT mission in 2009 and the lack of available and continuous Ku-band scatterometer retrievals has made it a high priority to ensure the compatibility of QuikSCAT and the continuing C-band ASCAT mission measurements. Yet examination of collocated observations during a 13 month period of mission overlap November 2008–November 2009 shows that there are systematic differences in the 10 m neutral wind estimates from the two missions. This study is an attempt to identify and model these differences in order to produce a consistent scatterometer-based wind record spanning the period 1999 to present.

[33] The basic data set we use to identify the differences and develop corrections is the set of space-time collocated satellite wind observations from the two missions and triply collocated satellite-satellite-buoy observations during the 13 month period of overlap. Since the scatterometers have different orbits the first part of the study explores the acceptable range of spatial and temporal lags for comparison study. We find a high temporal correlation (≥0.8) for time lags of up to 4 h and thus 4 h was determined to be the maximum acceptable time separation for winds stronger than 3.5 m/s. Requiring shorter time lags severely limits the number of collocated observations at lower latitudes. Similarly, spatial separations of up to 50 km were determined to be acceptable.

[34] The second part of the study examines the collocated winds for systematic differences. An examination of the collocated winds shows a high degree of agreement in direction, but reveals systematic differences in speed that depend on rain rate, the strength of the wind, and SST. We find that the impact of rainfall on the higher frequency of the two scatterometers, QuikSCAT, introduces biases of up to 1 m s^{-1} in the tropical convergence zones and the high precipitation zones of the midlatitude storm tracks *even after* rain flagged data are removed. This 1 m s^{-1} bias is cut in half by removing QuikSCAT wind retrievals with multidimensional rain probabilities > 0.05 even though this additional rain flagging reduces data amount by only 5%. For this reason we recommend the additional rain flagging.

[35] We next examine the causes of the differences in collocated wind speed remaining after removing QuikSCAT winds with MRP > 0.05. Data shown in Figures 3–6 suggest that QuikSCAT and ASCAT wind directions are consistent.

Wind speed difference from the two instruments is a function of ASCAT wind speed and direction relative to the mid-beam azimuth, but it is virtually independent of the ASCAT incident angle, a dependence strongly suggesting bias in the ASCAT geophysical model function. We model this dependence based on our analysis of the collocation data, and is then remove the dependence. Use of this bias model reduces collocated differences by 0.5 m s^{-1} in the tropics where it has large scale patterns related to variability of wind speed and direction.

[36] After applying the above two corrections, a third source of difference is evident in that QuikSCAT wind speed remains systematically lower (by 0.5 m s^{-1}) than ASCAT wind speed at high latitudes where SST < 5°C. An examination of the physics of centimeter-scale wind waves implicates the SST-dependence of wave dissipation, an effect which is enhanced for shorter waves. Again, the higher frequency scatterometer, QuikSCAT, will be more sensitive to this effect.

[37] Two additional sources of differences in the collocated observations are also identified. Differences in wind retrievals occur in storm track zones due to underestimation of infrequent strong wind events (>20 m s^{-1}) by ASCAT. Differences in wind speed estimates are also evident in the Peruvian and Namibian coastal zones where diurnal land-sea breezes are poorly resolved by the time delays between successive passes of the two scatterometers (up to 4 h in this study). Thus these latter differences seem to be a result of the limitations of the collocated data rather than indicating error in the scatterometer winds.

Appendix A: Impact of SST on the Bragg Scattering

[38] The purpose of this appendix is to evaluate deviation in retrieved scatterometer wind speed due to changes in SST. This evaluation is done for the pure Bragg scattering and using simplified model of the Bragg wave spectrum.

[39] Radar backscatter, σ^0, is mostly affected by energy of the resonant Bragg wave component. According to *Donelan and Pierson* [1987] for the pure Bragg scattering regime radar backscatter σ^0 is a positive definite function of the spectrum of the resonant Bragg wave component whose energy depends on the balance of wind wave growth parameter β_w and viscous dissipation β_ν that is a function of SST, $\sigma^0 = F(\beta_w - \beta_\nu)$. For simplicity, we next consider waves aligned with wind and use the *Plant* [1982] parameterization $\beta_w = \rho_a/\rho_w C_\beta (u_*/c)^2$ where c is the Bragg wave phase speed, ρ_a/ρ_w is the air to water density ratio, $C_\beta = 32$ is an empirical constant, $u_* = \sqrt{C_D}W$ is the friction velocity in the air, C_D is the neutral drag coefficient that is parameterized following *Large and Yeager* [2009]. This β_w works over wide range of u_*/c but fails at small values corresponding to threshold winds [*Donelan and Pierson*, 1987]. It should be also corrected by a factor $(1 - \alpha_c)$, where α_c is the wind-wave coupling parameter to account for the splitting of total wind stress in the wave boundary layer into wave-induced and turbulent components [*Makin and Kudryavtsev*, 1999; *Kudryavtsev et al.*, 1999)

$$\beta_w = \rho_a/\rho_w C_\beta (u_*/c)^2 (1 - \alpha_c), \qquad (A1)$$

[40] Viscous dissipation, $\beta_\nu = 4\nu k^2 \omega^{-1}$, depends on the wave number, k, and frequency, ω, of the Bragg component. It also depends on the water temperature, T, through the kinematic viscosity, $\nu(T)$, that explains temperature behavior of the wind-wave growth threshold wind speed [*Donelan and Pierson*, 1987; *Donelan and Plant*, 2009]. We also assume that scatterometer calibration, $\sigma^0(W)$, corresponds to the globally and time mean sea surface temperature $T_0 = 19°C$. Then an expected error in retrieved wind speed $\tilde{W}$ due to deviation of local temperature from T_0, $\Delta T = T - T_0$, is calculated by differentiating along $\beta(T, W) = const$, i.e., SST-induced changes in radar backscatter, $\partial \sigma^0 / \partial \beta * \partial \beta / \partial T * \Delta T$, are interpreted as changes in retrieved wind speed $-\partial \sigma^0 / \partial \beta * \partial \beta / \partial W * \tilde{W}$:

$$\tilde{W}(k) = -\frac{\partial\beta/\partial T}{\partial\beta/\partial W}\Delta T = \frac{\Delta\rho_a/\rho_a\beta_w - \Delta\beta_\nu}{\partial\beta_w/\partial W}, \quad (A2)$$

where it is assumed/used that air temperature equals SST, only ρ_a in (A1) depends on temperature, and $\partial \beta_\nu/\partial W = 0$. The first term in (A2) accounts for changes in retrieved wind speed due to changes in the air density [*Bourassa et al.*, 2010]. For chosen β_w parameterization (A1) this term doesn't depend on k, thus doesn't contribute to the wind difference between Ku- and C-band. Temperature dependent difference between QS and AS winds is explained by the viscous term in (A2)

$$\delta W = \tilde{W}(k_{QS}) - \tilde{W}(k_{AS}) = -\frac{2\Delta\nu(\omega_{QS} - \omega_{AS})}{(\rho_a/\rho_w)C_\beta C_D W(1 - \alpha_c)}, \quad (A3)$$

where $\Delta\nu = \nu(T) - \nu(T_0)$.

References

Atlas, R., R. N. Hoffman, J. Ardizzone, S. M. Leidner, J. C. Jusem, D. K. Smith, and D. Gombos (2011), A cross-calibrated, multiplatform ocean surface wind velocity product for meteorological and oceanographic applications, *Bull. Am. Meteorol. Soc.*, 92, 157–174, doi:10.1175/2010BAMS2946.1.

Bentamy, A., K. B. Katsaros, M. Alberto, W. M. Drennan, and E. B. Forde (2002), Daily surface wind fields produced by merged satellite data, in *Gas Transfer at Water Surfaces*, *Geophys. Monogr. Ser.*, vol. 127, edited by M. A. Donelan et al., pp. 343–349, AGU, Washington, D. C., doi:10.1029/GM127p0343.

Bentamy, A., H.-L. Ayina, P. Queffeulou, and D. Croize-Fillon (2007), Improved near real time surface wind resolution over the Mediterranean Sea, *Ocean Sci.*, 3, 259–271, doi:10.5194/os-3-259-2007.

Bentamy, A., D. Croize-Fillon, and C. Perigaud (2008), Characterization of ASCAT measurements based on buoy and QuikSCAT wind vector observations, *Ocean Sci.*, 4, 265–274, doi:10.5194/os-4-265-2008.

Blanke, B., S. Speich, A. Bentamy, C. Roy, and B. Sow (2005), Modeling the structure and variability of the southern Benguela upwelling using QuikSCAT wind forcing, *J. Geophys. Res.*, 110, C07018, doi:10.1029/2004JC002529.

Bourassa, M. A., D. M. Legler, J. J. O'Brien, and S. R. Smith (2003), SeaWinds validation with research vessels, *J. Geophys. Res.*, 108(C2), 3019, doi:10.1029/2001JC001028.

Bourassa, M. A., E. Rodriguez, and R. Gaston (2010), NASA's Ocean Vector Winds science team workshops, *Bull. Am. Meteorol. Soc.*, 91, 925–928, doi:10.1175/2010BAMS2880.1.

Bourlès, B., et al. (2008), The Pirata program: History, accomplishments, and future directions, *Bull. Am. Meteorol. Soc.*, 89, 1111–1125, doi:10.1175/2008BAMS2462.1.

Donelan, M. A., and W. J. Pierson Jr. (1987), Radar scattering and equilibrium ranges in wind-generated waves with application to scatterometry, *J. Geophys. Res.*, 92, 4971–5029, doi:10.1029/JC092iC05p04971.

Donelan, M. A., and W. J. Plant (2009), A threshold for wind-wave growth, *J. Geophys. Res.*, 114, C07012, doi:10.1029/2008JC005238.

Dunbar, S., et al. (2006), QuikSCAT science data product user manual, version 3.0, *Doc. D-18053—Rev A*, Jet Propul. Lab., Pasadena, Calif. [Available at ftp://podaac-ftp.jpl.nasa.gov/allData/quikscat/L2B/docs/QSUG_v3.pdf.]

Ebuchi, N. (2011), Self-consistency of marine surface wind vectors observed by ASCAT, *IEEE Trans. Geosci. Remote Sens.*, 99, 1–8, doi:10.1109/TGRS.2011.2160648, in press.

Ebuchi, N., H. C. Graber, and M. J. Caruso (2002), Evaluation of wind vectors observed by QuikSCAT/SeaWinds using ocean buoy data, *J. Atmos. Oceanic Technol.*, 19, 2049–2062, doi:10.1175/1520-0426(2002)019<2049:EOWVOB>2.0.CO;2.

Fairall, C. W., E. F. Bradley, J. E. Hare, A. A. Grachev, and J. B. Edson (2003), Bulk parameterization of air-sea fluxes: Updates and verification for the COARE algorithm, *J. Clim.*, 16, 571–591, doi:10.1175/1520-0442(2003)016<0571:BPOASF>2.0.CO;2.

Freilich, M. H. (1997), Validation of vector magnitude data sets: Effects of random component errors, *J. Atmos. Oceanic Technol.*, 14, 695–703, doi:10.1175/1520-0426(1997)014<0695:VOVMDE>2.0.CO;2.

Grima, N., A. Bentamy, K. Katsaros, and Y. Quilfen (1999), Sensitivity of an oceanic general circulation model forced by satellite wind stress fields, *J. Geophys. Res.*, 104, 7967–7989, doi:10.1029/1999JC900007.

Grodsky, S. A., and J. A. Carton (2001), Coupled land/atmosphere interactions in the West African monsoon, *Geophys. Res. Lett.*, 28, 1503–1506, doi:10.1029/2000GL012601.

Houze, R. A., and C.-P. Cheng (1977), Radar characteristics of tropical convection observed during GATE: Mean properties and trends over the summer season, *Mon. Weather Rev.*, 105, 964–980, doi:10.1175/1520-0493(1977)105<0964:RCOTCO>2.0.CO;2.

Kudryavtsev, V., V. Makin, and B. Chapron (1999), Coupled sea surface-atmosphere model: 2. Spectrum of short wind waves, *J. Geophys. Res.*, 104, 7625–7639, doi:10.1029/1999JC900005.

Kudryavtsev, V., D. Akimov, J. Johannessen, and B. Chapron (2005), On radar imaging of current features: 1. Model and comparison with observations, *J. Geophys. Res.*, 110, C07016, doi:10.1029/2004JC002505.

Large, W. G., and S. G. Yeager (2009), The global climatology of an interannually varying air-sea flux data set, *Clim. Dyn.*, 33, 341–364, doi:10.1007/s00382-008-0441-3.

Locarnini, R. A., A. V. Mishonov, J. I. Antonov, T. P. Boyer, H. E. Garcia, O. K. Baranova, M. M. Zweng, and D. R. Johnson (2010), *World Ocean Atlas 2009*, vol. 1, *Temperature*, *NOAA Atlas NESDIS*, vol. 68, NOAA, Silver Spring, Md.

Makin, V., and V. Kudryavtsev (1999), Coupled sea surface–atmosphere model: 1. Wind over waves coupling, *J. Geophys. Res.*, 104, 7613–7623, doi:10.1029/1999JC900006.

McPhaden, M. J., et al. (1998), The tropical ocean–global atmosphere observing system: A decade of progress, *J. Geophys. Res.*, 103, 14,169–14,240, doi:10.1029/97JC02906.

McPhaden, M. J., et al. (2009), RAMA: The Research Moored Array for African-Asian-Australian Monsoon Analysis and Prediction, *Bull. Am. Meteorol. Soc.*, 90, 459–480, doi:10.1175/2008BAMS2608.1.

Meindl, E. A., and G. D. Hamilton (1992), Programs of the National Data Buoy Center, *Bull. Am. Meteorol. Soc.*, 4, 984–993.

Milliff, R. F., W. G. Large, J. Morzel, G. Danabasoglu, and T. M. Chin (1999), Ocean general circulation model sensitivity to forcing from scatterometer winds, *J. Geophys. Res.*, 104(C5), 11,337–11,358, doi:10.1029/1998JC900045.

Plant, W. J. (1982), A relationship between wind stress and wave slope, *J. Geophys. Res.*, 87(C3), 1961–1967, doi:10.1029/JC087iC03p01961.

Ricciardulli, L., and F. Wentz (2011), Reprocessed QuikSCAT (V04) wind vectors with Ku-2011 geophysical model function, *Tech. Rep. 043011*, Remote Sens. Syst., Santa Rosa, Calif.

Risien, C. M., and D. B. Chelton (2008), A global climatology of surface wind and wind stress fields from eight years of QuikSCAT scatterometer data, *J. Phys. Oceanogr.*, 38, 2379–2413, doi:10.1175/2008JPO3881.1.

Rolland, J., and P. Blouch (2002), Les bouées météorologiques, *Meteorol.* 39, Meteo France, Paris. [Available at http://documents.irevues.inist.fr/bitstream/handle/2042/36252/meteo_2002_39_83.pdf.]

Sobieski, P. W., C. Craeye, and L. F. Bliven (1999), Scatterometric signatures of multivariate drop impacts on fresh and salt water surfaces, *Int. J. Remote Sens.*, 20, 2149–2166, doi:10.1080/014311699212164.

Tournadre, J., and Y. Quilfen (2003), Impact of rain cell on scatterometer data: 1. Theory and modeling, *J. Geophys. Res.*, *108*(C7), 3225, doi:10.1029/2002JC001428.

Verspeek, J., A. Stoffelen, M. Portabella, H. Bonekamp, C. Anderson, and J. F. Saldana (2010), Validation and calibration of ASCAT using CMOD5.n, *IEEE Trans. Geosci. Remote Sens.*, *48*, 386–395, doi:10.1109/TGRS.2009.2027896.

Weissman, D. E., M. A. Bourassa, and J. Tongue (2002), Effects of rain rate and wind magnitude on SeaWinds scatterometer wind speed errors, *J. Atmos. Oceanic Technol.*, *19*, 738–746, doi:10.1175/1520-0426(2002) 019<0738:EORRAW>2.0.CO;2.

Wright, J. W., and W. C. Keller (1971), Doppler spectra in microwave scattering from wind waves, *Phys. Fluids*, *14*, 466–474, doi:10.1063/1.1693458.

Zhang, H.-M., J. J. Bates, and R. W. Reynolds (2006), Assessment of composite global sampling: Sea surface wind speed, *Geophys. Res. Lett.*, *33*, L17714, doi:10.1029/2006GL027086.

A. Bentamy, B. Chapron, and D. Croizé-Fillon, Institut Francais pour la Recherche et l'Exploitation de la Mer, Plouzane F-29280, France.

J. A. Carton and S. A. Grodsky, Department of Atmospheric and Oceanic Science, University of Maryland, College Park, MD 20742, USA. (senya@atmos.umd.edu)